Unraveling Salt-Responsive Genes in Suaeda salsa through Genomic and Transcriptomic Profiling across Salinity Gradients

Min Li
Wayne State University
Xiangyu Zhou
Wayne State University
Jiaxin Wu
Shanghai Ocean University
Edward M. Golenberg
Wayne State University
Dongxiao Zhu
Wayne State University
Peimin He
Shanghai Ocean University
Chuanzhu Fan
cfan@wayne.edu
Wayne State University

Research Article

Keywords: Suaeda salsa, salinity, growth, halophyte, genome annotation, transcriptome

Posted Date: October 23rd, 2025

DOI: https://doi.org/10.21203/rs.3.rs-7624788/v1

Additional Declarations: No competing interests reported.

Version of Record: A version of this preprint was published at BMC Genomics on April 10th, 2026. See the published version at https://doi.org/10.1186/s12864-026-12825-5.

Unraveling Salt-Responsive Genes in *Suaeda salsa* through Genomic and Transcriptomic Profiling across Salinity Gradients

Min Li[a,b], Xiangyu Zhou[c], Jiaxin Wu[b], Edward M. Golenberg[a], Dongxiao Zhu[c], Peimin He[b*], and Chuanzhu Fan[a*]

[a] *Department of Biological Sciences, Wayne State University, Detroit, MI 48202, USA*

[b] *College of Oceanography and Ecological Science, Shanghai Ocean University, Shanghai 201306, China*

[c] *Department of Computer Sciences, Wayne State University, Detroit, MI 48202, USA*

*Corresponding authors.

E-mail addresses: pmhe@shou.edu.cn (P. He), cfan@wayne.edu (C. Fan)

ABSTRACT

Salinity severely limits global crop productivity, prompting a need to uncover plant salinity adaptation strategies. *Suaeda salsa* (L.) Pall., a halophyte thriving in saline habitats, offers a valuable model to dissect plant growth mechanisms under saline conditions. Although *S. salsa* genome assembly was recently improved, the corresponding gene annotation remained unpublished. Using the Helixer tool, we generated and released the first publicly available genome annotation for *S. salsa*, exhibiting high completeness with 92.80% (1,498) complete BUSCOs, thus providing an essential genomic resource. Using the *S. salsa* genome and annotation as our references, we conducted RNA-seq based transcriptomic profiling of plants subjected to 0, 200, and 400 mM NaCl for 30 days, respectively. We identified 462 significantly differentially expressed annotated genes across all treatments, with 11 key candidates consistently regulated. These genes are involved in key salinity response related activities including ion transport, osmotic adjustment, antioxidant defense, hormone signaling, transcriptional regulation, and genome plasticity. Enrichment analyses further supported their roles in ion homeostasis, redox regulation, and metabolic adjustment. This study provides new

insights into *S. salsa*'s long-term salt tolerance mechanisms during normal development. The findings lay a foundation for future functional studies, comparative evolutionary analyses, and genetic improvement of salt-tolerant crops.

Key words: *Suaeda salsa*, salinity, growth, halophyte, genome annotation, transcriptome

Introduction

Soil salinity poses a major global challenge, significantly limiting plant growth, development, and agricultural productivity [1]. High soil salinity disrupts plant physiological homeostasis to inhibit normal growth by altering osmotic balance, disturbing ion homeostasis, and impairing critical metabolic pathways, often culminating in substantial reductions in crop yields [2]. Halophytes, plants adapted and grown in soil or water of high salinity, have evolved specialized physiological and molecular mechanisms allowing them not only to survive but also to thrive under saline environments [3].

Suaeda salsa (L.) Pall., an annual leaf-succulent halophyte, is extensively distributed across saline habitats in Eurasia and is cultivated commercially as a seawater-irrigated vegetable along coastal regions in China. Due to its remarkable capacity for vacuolar salt accumulation and sustained photosynthetic efficiency under high salinity, *S. salsa* has emerged as a significant model species for investigating halophytic stress tolerance mechanisms [4].

Previous studies have revealed several important physiological and molecular mechanisms that contribute to normal growth under saline environment in *S. salsa,* with hormonal regulation, efficient ion compartmentation, and osmotic adjustment being among the most critical [5]. For example, differential modulation of hormones such as abscisic acid (ABA) and gibberellins, along with the strategic sequestration of sodium ions within cellular vacuoles,

play essential roles in *S. salsa*'s remarkable salt tolerance [2]. Additionally, accumulation of compatible solutes like proline, glycine betaine, and other osmoprotectants enables effective osmotic adjustment, maintaining cellular water balance [6]. Correspondingly, decreased soluble sugar concentrations further contribute to osmotic homeostasis.

Functional genomic studies have identified several salt-responsive genes critical to physiological and ecological salinity adaptations in *S. salsa*. For example, when expressed in *Arabidopsis thaliana*, genes encoding glycerol-3-phosphate acyltransferase (GPAT) and vacuolar H^+/Ca^{2+} transporters significantly enhance salt tolerance [7, 8]. Aquaporins, critical plasma membrane channel proteins, regulate water uptake and are central to maintaining leaf succulence under saline conditions [6]. Genes associated with osmolyte biosynthesis, such as myo-inositol-1-phosphate synthase (INPS), choline monooxygenase (CMO), and betaine aldehyde dehydrogenase (BADH), show robust upregulation under salt stress, indicating their roles in stress mitigation [5, 9]. Enhanced expression of antioxidative enzymes, including catalase (CAT) and superoxide dismutase (SOD), further demonstrate active management of reactive oxygen species (ROS) in response to salinity [6].

Metabolomic studies of *S. salsa* have revealed extensive metabolic reprogramming under salt conditions, marked by increased accumulation of protective metabolites such as glycine betaine, proline, and allantoin, accompanied by reductions in specific amino acids and sugars [6]. Comparative transcriptomic analyses among halophytes further these adaptive patterns, highlighting conserved induction of expansin proteins, protein phosphatases, ethylene signaling genes, WRKY transcription factors, and fatty acid desaturases in salt-tolerant species such as *Suaeda glauca* [9], *Gossypium hirsutum* and *Phaseolus vulgaris* [10].

Despite these insights, the availability of comprehensive genomic resources and integrated transcriptomic analyses for *S. salsa* remains limited. Although the genome of *S. salsa* has been published and is accessible through a public database [11], a high-quality, publicly available genome annotation has been lacking, significantly hindering in-depth functional genomic research. To address this gap, we generated the first comprehensive genome annotation for *S. salsa* (in GFF3 format), which is now publicly available via the NCBI database, providing a valuable resource for halophyte genomics research. Using this *S. salsa* genome and annotation as references, we conducted RNA-seq based transcriptomic analyses across multiple salinity treatments to uncover widespread and significant salt-responsive gene expression changes. Through these rigorous analyses, we identified 11 candidate genes that are significantly and highly upregulated or downregulated in response to salinity, suggesting their pivotal roles to maintain normal growth in the adaptive mechanisms underlying salt tolerance.

Collectively, our comprehensive genomic and transcriptomic framework offers novel insights into the molecular mechanisms of salt tolerance in *S. salsa* and provides a robust genomic framework for future functional and comparative genomic studies. These advancements pave the way for leveraging halophyte-derived genetic resources to enhance salt tolerance in economically important crops, addressing critical agricultural challenges posed by soil salinization.

Results

Sequencing Data and Read Mapping Statistics

A total of nine RNA-seq libraries from *S. salsa* were sequenced, generating between 43.9 and 50.8 million clean reads per sample (Table S1). The sequencing achieved high-quality bases,

with Q20 scores exceeding 99% and Q30 scores around 97%, demonstrating the robustness of sequencing data. The average GC content ranged from 42.48% to 42.69%, consistent across samples and indicative of sequencing uniformity.

Cleaned RNA-seq reads were aligned to the reference genome using STAR. Each sample yielded an average mapped read length of approximately 148 bp. The unique mapping rate ranged from 84.70% to 85.22%, indicating a high degree of specificity in the mapping process. Multi-mapped reads accounted for 7.27% to 7.88%, while unmapped reads due to short lengths remained stable between 7.10% and 7.47%. Overall, these results highlight high sequencing quality and good compatibility of the transcriptomic reads with the recently assembled and annotated *S. salsa* reference genome (Table 1).

Genome and Genome Annotation

The RNA-seq reads were aligned to the *S. salsa* reference genome (GenBank accession: JBEUWQ000000000.1), recently released by Cui [11]. A gene structure prediction based on the *S. salsa* reference genome was independently performed using Helixer [12], resulting in the first publicly accessible GFF3 annotation for *S. salsa*. A total of 26,035 protein-coding genes, each represented by a single predicted transcript, were identified. Although this simplified representation likely captures the primary isoforms, future integration of long-read transcriptomic data could enhance the annotation by identifying alternative splice variants. BUSCO analysis (v5.8.2) performed on the predicted protein sequences using the embryophyta_odb10 lineage dataset identified 92.8% complete**,** 1.5% fragmented, and 5.6% missing BUSCOs out of 1,614 groups, indicating high annotation completeness (Table 2). The high unique transcriptomic mapping rates observed across samples (84.70 – 85.22%) further

highlight the excellent sequencing quality and strong compatibility between the transcriptomic data and the newly assembled and annotated reference genome.

Principal Component Analysis of Salinity Responses

To evaluate the global transcriptional landscape and assess the quality of RNA-seq data, we performed a series of multivariate analyses. Principal Component Analysis (PCA) revealed clear separation among samples according to salinity treatment (Fig. 1A), with PC1 and PC2 accounting for 55.93% and 26.07% of the variance, respectively.

The permutational multivariate analysis of variance, based on Euclidean distances from variance-stabilized counts, showed that salinity treatment explains a significant proportion of expression variance ($R^2 = 0.738$, $F = 8.4484$, $p = 0.007$), with low intra-group dispersion (Table S2). These results support the biological validity and statistical robustness of our design.

Hierarchical clustering of the top 1,000 most variable genes (Fig. 1B) further distinguished the transcriptomic profiles of each treatment group, while maintaining strong coherence among replicates. Notably, the SS3 replicates showed a slightly greater dispersion compared to SS1 and SS2, which may reflect intrinsic biological variability or potential transcriptomic responses to high salinity levels. Pearson correlation heatmaps (Fig. 1C) showed uniformly high correlations between biological replicates ($r > 0.94$, $p < 0.001$), underscoring data reliability. In addition, boxplots of variance-stabilized expression values (Fig. 1D) displayed consistent global expression distributions across all samples, confirming the overall integrity of the dataset for subsequent differential expression analysis.

Differentially Expressed Genes Identification

To investigate the transcriptional dynamics of *S. salsa* in response to salinity, we performed pairwise comparisons of gene expression across three NaCl concentrations: 0 mM (SS1, control), 200 mM (SS2), and 400 mM (SS3). Differential expression analysis using DESeq2 revealed a substantial reprogramming of gene expression under salt conditions. A total of 4,173 differentially expressed genes (DEGs) were identified between SS2 and SS1, including 2,721 upregulated and 1,452 downregulated genes (Table S3). In the SS3 vs SS1 comparison, 3,101 DEGs were found, with 1,991 upregulated and 1,110 downregulated (Table S4). The SS3 vs SS2 comparison yielded 2,712 DEGs, consisting of 1,347 upregulated and 1,365 downregulated genes (Table S5).

To visualize the global expression dynamics in response to salinity, we analyzed the union of DEGs identified from the SS2 vs SS1 and SS3 vs SS1 comparisons, which reflect transcriptomic changes relative to the no-salt control. A total of 4,173 and 3,101 DEGs were detected in SS2 vs SS1 and SS3 vs SS1, respectively, with an overlap of 1,894 genes between the two comparisons. After removing duplicates, the union set contained 5,380 unique DEGs, which were used for downstream visualization. Variance-stabilized transformation (VST) was applied to the raw count matrix, and the expression matrix was subset to include only these DEGs. Genes were then ordered based on the average $\log_2$ fold change across both comparisons, and expression values were row-wise normalized using z-score transformation. A heatmap was generated to depict global expression patterns (Fig. 2A), revealing distinct clustering of samples according to salinity levels. SS2 and SS3 exhibited transcriptional profiles clearly separated from SS1, indicating both condition-specific and shared regulatory responses across increasing salinity concentrations.

A Venn diagram identified that 462 genes were consistently differentially expressed across all three comparisons (Fig. 2B). Gene Ontology enrichment analysis revealed the top 20 terms across the three major categories: Biological Process (BP), Molecular Function (MF), and Cellular Component (CC) (Fig. 2C). Notable BP terms included "cellular process" (GO:0009987), "metabolic process" (GO:0008152), and "response to stimulus" (GO:0050896); MF was dominated by "catalytic activity" (GO:0003824); and CC terms were enriched for "membrane" (GO:0016020), "cytoplasm" (GO:0005737), and related subcellular components. These results suggest that the DEGs are involved in core cellular functions, metabolic regulation, and stress responses, implicating their potential roles in salinity adaptation.

Identification key genes for *S. salsa* growth under saline conditions

To identify genes further and dissect the genetic basis of *S. salsa* growth under salt treatment, we conducted a targeted screening of the 462 commonly DEGs detected across all salinity treatments. From this set, we identified 11 genes whose expression levels exhibited a consistent trend in responses to increasing salinity and whose functional annotations are associated with known salt responses (Fig. 3). Among these, six genes (*chr2_001401.1*, *chr2_003131.1*, *chr3_000195.1*, *chr4_002858.1*, *chr6_000414.1*, *chr8_000327.1*) were significantly upregulated, whereas five genes (*chr2_000708.1*, *chr4_000776.1*, *chr5_000112.1*, *chr5_001889.1*, *chr7_001758.1*) showed substantial downregulation under salt stress conditions (Table 3).

Among the upregulated genes, *chr2_003131.1* encodes phosphoenolpyruvate carboxylase (PEPcase), a key enzyme involved in organic acid metabolism, osmotic adjustment, and ion homeostasis. Its enhanced expression under salinity stress aligns with previous findings in Arabidopsis and *Sorghum bicolor* L., where both transcript levels and enzymatic activities were

elevated in response to salt treatment. In Arabidopsis, PEPcase facilitates osmotic adjustment by promoting organic acid accumulation, thereby maintaining cellular osmotic balance and metabolic homeostasis (Sánchez et al., 2006). In *Sorghum bicolor*, RNAi-mediated knockdown of *SbPPC3* reduces salt tolerance [13], while salt stress induces PEPC kinase activity, leading to increased PEPcase phosphorylation [14]. These findings reinforce the conserved role of PEPcase in osmoprotectant biosynthesis and metabolic stabilization under saline conditions.

Chr3_000195.1 encodes a protein kinase potentially involved in the phosphorylation-mediated regulation of ion transport and stress-responsive signaling cascades, reminiscent of the functionally characterized SnRK2.4/2.10 and CBL-CIPK modules in Arabidopsis [15]. Additionally, metabolic enzymes such as RNase T2 (chr6_000414.1) and phosphoglycerate kinase (PGK; chr8_000327.1) exhibited upregulated expression under salinity. This is consistent with previous studies showing that T2/S-like ribonucleases, such as PvRNS3 in common bean, are induced by salt stress and contribute to stress adaptation through enhanced RNA turnover and nutrient recycling [16]. Likewise, overexpression of the PGK isoform OsPgk2a-P from the salt-tolerant rice cultivar Pokkali significantly improved salinity tolerance in transgenic tobacco by maintaining chlorophyll content, promoting proline accumulation, and stabilizing ion homeostasis, highlighting the critical role of PGK in energy metabolism under stress [17]. Notably, the significant induction of chr2_001401.1, encoding an LTR copia-type retrotransposon, many involving genomic plasticity through chromatin remodeling and transcriptional reprogramming. Similar mechanisms have been reported in *Zea mays* [18] and Arabidopsis [19], where LTR retrotransposons are activated by abiotic stress and shown to influence nearby gene expression.

Conversely, downregulated genes exhibited adaptations indicative of a shift from acute stress responses towards longer-term metabolic homeostasis. For example, *chr5_000112.1*, encoding galactinol synthase involved in raffinose family oligosaccharide (RFO) synthesis, exhibited suppressed expression. This may reflect a shift from early osmotic protection toward long-term metabolic adjustment. While salt-induced RFO accumulation has been reported in Arabidopsis [20], recent evidence in *Oryza sativa* shows that OsPP65 knockout leads to increased galactinol but decreased raffinose levels, suggesting a nuanced and dynamic regulation of RFO metabolism during salt stress adaptation [21]. *Chr5_001889.1*, encoding peroxidase (POD), was significantly downregulated under prolonged salt stress, potentially reflecting a shift or suppression in classical ROS-scavenging pathways. While peroxidase activity typically increases under salt stress in other species, such as *Solanum lycopersicum* [22], and *GsPRX9* expression was induced in *Glycine soja*, enhancing salt tolerance when overexpressed [23], the contrasting pattern observed in *S. salsa* may indicate species-specific or time-dependent antioxidant regulation. An alternative explanation is that the generation of ROS itself is reduced under prolonged salinity exposure, possibly due to a general slowdown or reprogramming of metabolic activity. In such conditions, the cellular demand for ROS-scavenging enzymes like POD would be reduced accordingly. This downregulation may represent an energy-conserving strategy adopted by *S. salsa* during long-term adaptation to saline environments.

Likewise, the downregulation of *chr7_001758.1*, encoding cysteine synthase, implies a potential reduction in sulfur assimilation and glutathione-mediated redox buffering during prolonged salt exposure. Interestingly, overexpression of cysteine synthase in *Medicago sativa* L. enhanced alkali tolerance by increasing cysteine, proline, and antioxidant activity, while foliar application of L-cysteine in *Linum usitatissimum* L. alleviated salt-induced oxidative stress.

These contrasting patterns suggest that cysteine-associated redox pathways may play context-dependent roles across species or stress types [24, 25]. Furthermore, *chr2_000708.1*, involved in ABA biosynthesis and the xanthophyll cycle, showed decreased expression indicative of a temporal modulation from acute ABA-mediated signaling towards sustained metabolic acclimation under prolonged salt exposure [26]. Distinct regulation patterns of transcription factors, including downregulated AP2/ERF (*chr4_000776.1*) and upregulated bZIP family genes (*chr4_002858.1*), underscore the complex transcriptional shifts orchestrating antioxidative, osmotic, and hormonal networks during salt stress adaptation [27, 28].

To further understand the functional significance of the identified DEGs, KEGG enrichment analysis and pathway–gene network construction were performed. Seven genes were annotated with KEGG Orthology (KO) identifiers, connecting them to 20 unique metabolic pathways (Fig. 4). This network analysis clearly delineated highly interconnected pathways including carbon metabolism, glycolysis/gluconeogenesis, glutathione metabolism, and sulfur metabolism, among others, reflecting crucial biological processes underpinning salt stress adaptation. Particularly, *chr7_001758.1* (cysteine synthase)**,** *chr8_000327.1* (phosphoglycerate kinase, and *chr2_003131.1* (phosphoenolpyruvate carboxylase) emerged as hub genes involved in multiple metabolic pathways, suggesting their central regulatory roles in orchestrating complex physiological responses under salinity conditions.

Discussion

Salinity significantly restricts plant growth, development, and agricultural productivity, necessitating sophisticated physiological and molecular adaptations [29]. In this study, we comprehensively characterized the transcriptional landscape of normal growth *S. salsa* plants

under incremental salinity conditions, leveraging the first publicly available genome annotation for this halophyte [11]. Our comprehensive transcriptomic RNA-seq analysis revealed extensive transcriptional reprogramming across a gradient of salinity, with 462 DEGs. Specifically, we identified 11 robust candidate genes that exhibited consistent trends (up- or down-regulation) with increasing salinity ($p < 0.05$, $\log_2|\text{Fold Change}| > 1$).

Our data reveal that *S. salsa* plants initially prioritize the stabilization of osmotic and energetic balance. The early upregulation of genes encoding PEPcase, PGK, and RNase T2 reflects a rapid deployment of metabolic and osmoprotectant mechanisms. PEPcase facilitates organic acid accumulation, contributing to cellular osmotic adjustment and ionic equilibrium, a conserved function observed in both *Arabidopsis thaliana* and *Sorghum bicolor* under salt stress [13, 14, 30]. PGK enhances glycolytic flux to sustain energy production, while RNase T2 promotes RNA turnover and phosphate recycling, supporting metabolic flexibility under resource-limiting conditions [16]. Together, these responses reflect a rapid shift in cellular priorities aimed at mitigating osmotic imbalance and ensuring energy supply for normal development of salinity-tolerance plants, like *S. salsa*.

As salinity persists, *S. salsa* enters a phase of deeper transcriptional reprogramming and genomic adaptation to continue normal growth. One of the most striking findings is the strong induction of an LTR copia-type retrotransposon, suggesting activation of transposable elements as a potential mechanism for enhancing genomic plasticity. Transposons are known to respond to environmental cues, reshaping local chromatin structure or modulating nearby gene expression, thereby contributing to long-term epigenomic flexibility and adaptive potential [18, 19]. The biological implications of this activation in *S. salsa* remain unclear but may reflect either a

stress-induced loosening of epigenetic repression or a deleterious side effect of prolonged environmental pressure.

In contrast, several downregulated genes reflect a shift from high-energy, acute defense responses to more energy-conservative, sustained tolerance mechanisms. Genes encoding galactinol synthase and cysteine synthase, key players in raffinose family oligosaccharide biosynthesis and sulfur assimilation, respectively, showed marked suppression under salinity. This may reflect a redirection of carbon and sulfur flux away from costly osmoprotectant and antioxidant production as *S. salsa* transitions into long-term acclimation [20, 21, 24, 25]. The downregulation of a peroxidase gene further suggests a possible shift in redox buffering systems, either through species-specific antioxidant strategies or temporal regulation of ROS detoxification [22, 23]. All these transcriptional downward shifts may promote salt-tolerance plants, i.e., *S. salsa* to accommodate these adverse conditions to maintain the optimal metabolism for development and growth.

Interestingly, the transcriptional control network also undergoes reprogramming. The suppression of AP2/ERF and ABA biosynthetic genes, coupled with the induction of a bZIP transcription factor, highlights a transition from transient hormonal signaling to a more stable, transcriptional control regime. Such a shift likely facilitates long-term adaptation by stabilizing stress-responsive gene expression programs while minimizing unnecessary hormonal fluctuation [26-28]. Pathway enrichment analysis further supports this phased model of adaptation. KEGG terms such as “carbon metabolism,” “plant hormone signal transduction,” and “glutathione metabolism” were significantly enriched among DEGs, underscoring the integrated nature of energy homeostasis, hormonal crosstalk, and redox regulation in *S. salsa*. These networks

collectively orchestrate a systemic response that balances immediate defense with long-term plasticity.

In summary, our findings reveal a temporally structured, multi-tiered adaptation strategy in *S. salsa*, encompassing rapid metabolic defense, epigenomic reprogramming, and sustained transcriptional control for their development and growth under salinity environments. The identified candidate genes offer promising entry points for dissecting halophyte resilience and provide valuable molecular resources for engineering salinity tolerance in crop species. As soil salinization continues to threaten arable lands globally, understanding the natural stress-adaptive repertoire of halophytes like *S. salsa* may inform future solutions for sustainable agriculture and ecosystem restoration. While qRT-PCR validation was not performed in this study, our previous experiments have confirmed the reliability of our RNA-seq pipeline [31]. Future investigations will benefit from spatiotemporal validation of these candidate genes and functional assays, such as CRISPR/Cas9-mediated mutagenesis, overexpression analysis, and epigenetic profiling to elucidate the mechanistic roles of these regulators in salinity adaptation. Additionally, incorporating time-series transcriptomic analyses will help capture the dynamic trajectory of stress responses and reveal stage-specific regulatory mechanisms.

Materials and methods

Plant Growth and Sample Collection

Suaeda salsa seeds were sourced from Suqian City, Jiangsu Province. After surface sterilization in 1% potassium permanganate for 20 min, seeds were rinsed thoroughly and imbibed in water for 24 hours. Seeds were then sown in perforated pots under controlled conditions (25 °C day/20 °C night, 600 μmol·m^{-2}·s^{-1} light intensity, 14 h light/10 h dark photoperiod) and irrigated daily with half-strength Hoagland nutrient solution containing 100

mmol·L^{-1} NaCl. The detailed composition of the nutrient solution is described in our previous work [31]. Seedlings of *S. salsa* were first germinated and grown under uniform, non-saline conditions until they developed six pairs of true leaves. At this stage, plants were assigned to three treatment groups designated as SS1, SS2, and SS3, corresponding to salinity levels of 0, 200, and 400 mM NaCl, respectively. The salt treatments were maintained for 30 consecutive days. After 30 days of salinity treatment, leaf tissues from the upper third of each plant were harvested for RNA extraction and transcriptome sequencing.

Source of Genome and Genome Annotation

The reference genome of *S. salsa* used in this study was downloaded from the NCBI database (BioProject: PRJNA1125603; BioSample: SAMN41901509; GenBank accession: JBEUWQ000000000.1), uploaded by Cui [11] as part of a whole genome shotgun sequencing project.

As no official GFF annotation was available, gene annotation was performed using a GFF3 file predicted by Helixer v0.3.4 [12]. This annotation was used for read summarization and gene-level quantification. The -g ID parameter was specified during count matrix generation to group transcript features by gene ID. To evaluate the completeness of the Helixer-derived gene annotation, BUSCO v5.8.2 [32]was run on the predicted protein sequences using the *embryophyta_odb10* lineage dataset (2025-06-19).

Genome indexing was performed using STAR v2.7.11b [33] with the genome FASTA file and the Helixer-generated GFF3 annotation. STAR indices were generated using the parameters --sjdbOverhang 99 and --sjdbGTFtagExonParentTranscript Parent, which optimize spliced alignment for GFF3-formatted annotations.

RNA extraction, library construction and high-throughput Illumina sequencing

Total RNA was extracted from tissue samples and sequenced by Majorbio Co., Ltd. (Shanghai, China). Three biological replicates were included for each treatment. RNA quality was rigorously assessed using multiple approaches: concentration and purity were measured with a Nanodrop 2000 spectrophotometer, integrity was evaluated by agarose gel electrophoresis, and RNA Quality Number (RQN) was determined using the Agilent 5300 Fragment Analyzer. Only RNA samples meeting the following strict criteria were used for library construction: total RNA quantity ≥ 1 μg, concentration ≥ 30 ng/μL, RQN > 6.5, and OD260/280 ratio between 1.8 and 2.2.

Polyadenylated mRNAs were isolated from total RNA using oligo(dT)-conjugated magnetic beads, which selectively bind to the poly(A) tails of eukaryotic mRNAs. The purified mRNA was then fragmented into ~300 bp fragments using fragmentation buffer under controlled conditions to suit short-read sequencing requirements. First-strand cDNA was synthesized using random primers and reverse transcriptase, followed by second-strand synthesis to generate double-stranded cDNA. End-repair was then performed to produce blunt ends, and a single 'A' nucleotide was added to the 3′ ends to facilitate adapter ligation.

Adapter-ligated cDNA fragments were purified and size-selected, followed by PCR amplification to enrich for successfully ligated fragments. The final libraries were quantified using a Qubit 4.0 fluorometer, pooled based on target sequencing depth, and subjected to cluster generation via bridge amplification on the Illumina cBot system. Paired-end (2 × 150 bp) sequencing was performed on the Illumina NovaSeq 6000 platform according to the manufacturer's standard protocol.

RNA-seq Data Processing and Gene Expression Quantification

Raw paired-end RNA-seq reads generated by the NovaSeq platform were first trimmed using Cutadapt v4.9 [34] to remove Illumina universal adapter sequences (*AGATCGGAAGAG*) from both forward and reverse reads. Reads shorter than 25 bp after trimming were discarded. The quality of the trimmed reads was assessed using FastQC v0.11.8 [35] to ensure sequencing integrity. For each sample, trimmed paired-end reads were concatenated prior to alignment.

Reads were aligned to the reference genome using STAR with the options --outSAMstrandField intronMotif and --outSAMunmapped Within to retain splicing junctions and unmapped read information. The resulting SAM files were converted to BAM format, sorted, and indexed using samtools v1.9 [36]. Gene-level quantification was performed using featureCounts from the Subread package v2.0.6 [37], based on the Helixer-generated GFF3 annotation file. The resulting raw count matrix was used for downstream differential expression analysis using the DESeq2 package [38] in R (v4.2.2).

RNA-seq Quality Control and Multivariate Statistical Analysis

To assess the consistency and global structure of the RNA-seq dataset across treatments, we applied a series of multivariate analyses using R. Variance-stabilizing transformation (VST), which was performed on raw count data using DESeq2. And the transformed values were subsequently used for downstream visualization and statistical testing. Principal Component Analysis (PCA) was conducted using the plotPCA() function from DESeq2 to reduce dimensionality and visualize sample clustering. The top 500 most variable genes across all samples were included in the PCA calculation. The first two principal components (PC1 and

PC2), which together explained >80% of the variance, were plotted to illustrate inter- and intra-group sample separation.

To statistically validate the PCA-based groupings, we performed a permutational multivariate analysis of variance (PERMANOVA) using the adonis2() function in the vegan package v2.6.10 [39].

Hierarchical clustering was conducted on the top 1,000 most variable genes using Euclidean distance and complete linkage. Clustering results were visualized with a heatmap generated using the pheatmap() function from the pheatmap package v1.0.12 [40], and rows/columns were scaled to highlight variation across treatments.

Sample-to-sample Pearson correlation analysis was performed using the cor() function and hierarchical clustering to evaluate reproducibility among biological replicates. All pairwise correlation coefficients ($r > 0.94$) indicated high data quality. Statistical significance, assessed with the cor.test() function (based on the Fisher transformation), confirmed that all correlations were highly significant ($p < 0.001$).

Finally, expression distributions across all samples were visualized via boxplots of VST values using base R functions, confirming that global gene expression levels were evenly distributed and free of batch effects.

Differential Expression Analysis and Functional Annotation

Downstream analyses were conducted in R contributed packages. Gene expression count matrices were filtered and processed using DESeq2. Count values from three biological replicates under each condition (SS1, SS2, SS3) were combined and aggregated by gene ID. Redundant gene IDs were merged by summing their counts using the summarise() function from

dplyr v1.1.4. Differential gene expression analysis was performed using DESeq2 with the model formula ~ condition. Genes were considered significantly differentially expressed if they met the thresholds of adjusted p.adj < 0.05 (two-tailed test) and $\log_2$|Fold Change| > 1.

To visualize global transcriptional patterns induced by salinity treatments relative to the control (0 mM NaCl), we compiled a union set of significantly differentially expressed genes (DEGs) from the SS2 vs SS1 (200 mM vs 0 mM) and SS3 vs SS1 (400 mM vs 0 mM) comparisons. This resulted in a total of 5,380 unique DEGs after removing overlapping genes. Variance-stabilized transformation (VST) was applied to the raw count matrix using the vst() function in DESeq2 (with blind = FALSE) to normalize expression values and reduce heteroscedasticity. The transformed expression matrix was then subset to include only the 5,380 DEGs.

To emphasize gene-level expression dynamics across treatments, we calculated the average $\log_2$ fold change for each gene across the two comparisons (SS2 vs SS1 and SS3 vs SS1) and used this metric to order genes from lowest to highest. Z-score normalization was applied row-wise to standardize expression values across samples for each gene. A heatmap was generated using the pheatmap package, with hierarchical clustering applied to columns (samples) but not to rows (genes), thereby preserving the predefined gene order. Treatment conditions were annotated above the columns to reflect sample grouping by salinity level.

To understand their functions, we performed a comprehensive annotation analysis of these DEGs using five databases: EggNOG mapper v2.1.12 [41], UniProt [42] (accessed April 2025), KEGG (accessed April 2025), RefSeq (accessed April 2025), and Gene Ontology. EggNOG mapper provided orthology-based functional assignments across multiple species. The

output annotation file (out.emapper.annotations) was parsed in R to extract Gene Ontology (GO) terms and KEGG ortholog (KO) identifiers.

GO enrichment analysis was conducted using the enricher () function in the clusterProfiler package v4.12.6 [43]. GO terms were reformatted into a two-column TERM2GENE data frame, associating GO terms with corresponding gene IDs. For each contrast group (SS1 vs SS2, SS1 vs SS3, SS2 vs SS3), significantly differentially expressed genes ($p < 0.05$ and $\log_2|\text{Fold Change}| > 1$) were used as input. Parameters were set to pvalueCutoff = 1, qvalueCutoff = 1, minGSSize = 1, and maxGSSize = 5000 to include all terms for exploratory visualization. Results were visualized using the dotplot() function from enrichplot v1.24.4. KEGG pathway enrichment followed the same framework. KO identifiers were extracted and split using the separate_rows() function from tidyr (v1.3.1), and a TERM2GENE data frame was constructed linking KO terms with gene IDs. KEGG enrichment was then performed using the same statistical thresholds.

All enrichment results were visualized as dot plots in R, and summary tables of enriched pathways were compiled for downstream interpretation. Gene Ontology (GO) enrichment analysis was also conducted, and only the top 20 significantly enriched GO terms (ranked by p.adj) were included in the final figure. For KEGG enrichment results, circular bubble plots representing pathway enrichment statistics were generated using the online platform OmicShare Tools [44]. In addition, GraphPad Prism version 10.4.2 (GraphPad Software, Inc.) was used to generate bar plots illustrating the expression patterns of selected DEGs across salinity gradients.

Conclusion

In summary, using the *S. salsa* reference genome, along with newly generated genome annotations and transcriptome data, this study identified 11 key salt-responsive genes involved in

ion transport, osmotic adjustment, antioxidant defense, and genome plasticity. These data resources and findings advance our understanding molecular mechanisms of plant growth under salinity tolerance and provide a valuable foundation for future crop improvement efforts.

Data Availability

The original RNA-Seq datasets have been deposited in the NCBI Sequence Read Archive and are publicly available under the accession number PRJNA1227148. The genome annotation data will be released upon publication of the paper.

Author's contributions

ML: Writing - Original Draft, Conceptualization, Methodology, Validation, Investigation, Formal analysis. XYZ: Software, Data Curation. JXW: Writing - Original Draft. EM. G: Formal analysis, Writing - Review and Editing. DXZ: Formal analysis, Data Curation, Writing - Review and Editing. PMH: Conceptualization, Resources, Writing - Review and Editing, Funding acquisition. CZF: Supervising, Data Curation, Conceptualization, Writing - Review and Editing.

Conflict of interest statement

The authors declare no conflict of interest.

Funding Declaration

This work was supported by the Open Fund of the Key Laboratory of Marine Ecological Monitoring and Restoration Technology of the Ministry of Natural Resources (MEMIRT202003) and Shanghai Lingang Coastal Marine Ecological Protection and Restoration Project (2201PD0001) to P.H.

Acknowledgments

We thank High Performance Computing (HPC) of Wayne State University for providing grid computing services.

Supporting data

Additional Supporting Information may be found in the online version of this article.

References

1. Zhang X, Yao Y, Li X, Zhang L, Fan S. Transcriptomic analysis identifies novel genes and pathways for salt stress responses in leaves. Sci Rep-Uk. 2020;10(1):4236.
2. Li T, Yang X, Sun H, Jing H, Bao S, Hu Y, et al. Competitive ion uptake and transcriptional regulation as a coordinated dual mechanism of NaCl-mediated cadmium detoxification in. Plant Physiol Bioch. 2025;224:109939.
3. Munns R, Day DA, Fricke W, Watt M, Arsova B, Barkla BJ, *et al*. Energy costs of salt tolerance in crop plants. New Phytol. 2020; 225(3):1072-1090.
4. Mann A, Lata C, Kumar N, Kumar A, Kumar A, Sheoran P. Halophytes as new model plant species for salt tolerance strategies. Front Plant Sci. 2023;14:1137211.
5. Wu H, Liu X, You L, Zhang L, Zhou D, Feng J, et al. Effects of Salinity on Metabolic Profiles, Gene Expressions, and Antioxidant Enzymes in Halophyte. J Plant Growth Regul. 2012;31(3):332-341.
6. Guo S, Tang Y, Chu H, Sun M, Xing J. Transcriptome sequencing revealed molecular mechanisms underlying tolerance of to saline stress. Plos One. 2019;14(7):e0219979.
7. Han N, Lan W, He X, Shao Q, Wang B, Zhao X. Expression of a Suaeda salsa Vacuolar H/CaTransporter Gene in Arabidopsis Contributes to Physiological Changes in Salinity. Plant Mol Biol Rep. 2012;30(2):470-477.
8. Sui N, Tian S, Wang W, Wang M, Fan H. Overexpression of Glycerol-3-Phosphate Acyltransferase from Improves Salt Tolerance in Arabidopsis. Front Plant Sci. 2017;8:1337.
9. Jin H, Dong D, Yang Q, Zhu D. Salt-Responsive Transcriptome Profiling of via RNA Sequencing. Plos One. 2016;11(3):e0150504.
10. Brankova L, Ivanov S, Alexieva V. The induction of microsomal NADPH:cytochrome P450 and NADH:cytochrome b(5) reductases by long-term salt treatment of cotton (*Gossypium hirsutum* L.) and bean (*Phaseolus vulgaris* L.) plants. Plant Physiol Biochem. 2007;45(9):691-695.
11. Cui B, Liu R, Yu Q, Guo J, Du X, Chen Z, *et al*. Combined genome and transcriptome provides insight into the genetic evolution of an edible halophyte adaptation to high salinity. Mol Ecol. 2024;34(15):e17457.
12. Stiehler F, Steinborn M, Scholz S, Dey D, Weber APM, Denton AK. Helixer: cross-species gene annotation of large eukaryotic genomes using deep learning. Bioinformatics. 2020;36(22-23):5291-5298.
13. de la Osa C, Pérez-López J, Feria AB, Baena G, Marino D, *et al*. of phosphoenolpyruvate carboxylase 3 negatively impacts growth, productivity, and responses to salt stress in sorghum (*Sorghum bicolor* L.). Plant J. 2022;111(1):231-249.
14. Echevaría E, Garcia-Mauriño S, Alvarez R, Soler A, Vidal J. Salt stress increases the Ca-independent phosphopyruvate carboxylase kinase activity in leaves. Planta. 2001;214(2):283-287.
15. McLoughlin F, Galvan-Ampudia CS, Julkowska MM, Caarls L, van der Does D, Laurière C, et al. The Snf1-related protein kinases SnRK2.4 and SnRK2.10 are involved in maintenance of root system architecture during salt stress. Plant J. 2012;72(3):436-449.
16. Diaz-Baena M, Galvez-Valdivieso G, Delgado-Garcia E, Pineda M, Piedras P. Nuclease and ribonuclease activities in response to salt stress: Identification of PvRNS3, a T2/S-

like ribonuclease induced in common bean radicles by salt stress. Plant Physiol Bioch. 2020;147:235-241.
17. Joshi R, Karan R, Singla-Pareek SL, Pareek A. Ectopic expression of Pokkali phosphoglycerate kinase-2 (OsPGK2-P) improves yield in tobacco plants under salinity stress. Plant Cell Rep. 2016;35(1):27-41.
18. Makarevitch I, Waters AJ, West PT, Stitzer M, Hirsch CN, Ross-Ibarra J, et al. Transposable Elements Contribute to Activation of Maize Genes in Response to Abiotic Stress. Plos Genet. 2015;11(1):e100415.
19. Jiao YL, Deng XW. A genome-wide transcriptional activity survey of rice transposable element-related genes. Genome Biol. 2007;8(2):R28.
20. Nishizawa A, Yabuta Y, Shigeoka S. Galactinol and raffinose constitute a novel function to protect plants from oxidative damage. Plant Physiol. 2008;147(3):1251-1263.
21. Liu Q, Ding J, Huang W, Yu H, Wu S, Li W, *et al*. Negatively Regulates Osmotic and Salt Stress Responses Through Regulating Phytohormone and Raffinose Family Oligosaccharide Metabolic Pathways in Rice. Rice. 2022;15(1):34.
22. Wu L, Jiang Q, Zhang Y, Du M, Ma L, Ma Y. Peroxidase Activity in Tomato Leaf Cells under Salt Stress Based on Micro-Hyperspectral Imaging Technique. Horticulturae. 2022;8(9):813.
23. Jin T, Sun Y, Zhao R, Shan Z, Gai J, Li Y. Overexpression of Peroxidase Gene GsPRX9 Confers Salt Tolerance in Soybean. Int J Mol Sci. 2019;20(15):3745.
24. Hussein HAA, Alshammari SO. Cysteine mitigates the effect of NaCl salt toxicity in flax (*Linum usitatissimum* L) plants by modulating antioxidant systems. Sci Rep-Uk. 2022;12(1):11359.
25. Yuan Y, Song T, Yu J, Zhang W, Hou X, Ling Z, et al. Genome-Wide Investigation of the Cysteine Synthase Gene Family Shows That Overexpression of Confers Alkali Tolerance to Alfalfa (*Medicago sativa* L.). Front Plant Sci. 2022;12:792862.
26. Ji X, Dong B, Shiran B, Talbot MJ, Edlington JE, Hughes T, et al. Control of Abscisic Acid Catabolism and Abscisic Acid Homeostasis Is Important for Reproductive Stage Stress Tolerance in Cereals. Plant Physiol. 2011;156(2):647-662.
27. Bakhtari B, Razi H, Alemzadeh A, Dadkhodaie A, Moghadam A. Identification and characterization of the Quinoa gene family and their expression patterns in response to salt stress. Sci Rep-Uk. 2024;14(1):29529.
28. Liu H, Tang X, Zhang N, Li S, Si H. Role of bZIP Transcription Factors in Plant Salt Stress. Int J Mol Sci. 2023;24(9):7893.
29. Li H, Wang H, Wen W, Yang G. The antioxidant system in Suaeda salsa under salt stress. Plant Signal Behav. 2020;15(7):1771939.
30. Sánchez R, Flores A, Cejudo F. phosphopyruvate carboxylase genes encode immunologically unrelated polypeptides and are differentially expressed in response to drought and salt stress. Planta. 2006;223(5):901-909.
31. Cai L, Li M, Shen Y, Jiang R, Wang J, Ma S, et al. Betacyanin accumulation mediates photosynthetic protection in *Suaeda salsa* (L.) Pall. under salt stress. Planta 2025;261(5):100.
32. Manni M, Berkeley MR, Seppey M, Simao FA, Zdobnov EM. BUSCO Update: Novel and Streamlined Workflows along with Broader and Deeper Phylogenetic Coverage for Scoring of Eukaryotic, Prokaryotic, and Viral Genomes. Mol Biol Evol. 2021;38(10):4647-4654.

33. Dobin A, Davis CA, Schlesinger F, Drenkow J, Zaleski C, Jha S, et al. STAR: ultrafast universal RNA-seq aligner. Bioinformatics. 2013;29(1):15-21.
34. Martin M. Cutadapt removes adapter sequences from high-throughput sequencing reads. EMBnet journal. 2011;17:10-12.
35. Andrews S. FastQC: a quality control tool for high throughput sequence data. 2010.
36. Li H, Handsaker B, Wysoker A, Fennell T, Ruan J, Homer N, et al. The Sequence Alignment/Map format and SAMtools. Bioinformatics. 2009;25(16):2078-2079.
37. Liao Y, Smyth GK, Shi W. FeatureCounts: an efficient general purpose program for assigning sequence reads to genomic features. Bioinformatics. 2014;30(7):923-930.
38. Love MI, Huber W, Anders S. Moderated estimation of fold change and dispersion for RNA-seq data with DESeq2. Genome Biol. 2014;15(12):550.
39. Oksanen J, Simpson GL, Blanchet FG, Kindt R, Legendre P, Minchin PR et al. Vegan: Community Ecology Package. R Package Version 2.6-4. 2022.
40. Kolde R. Pheatmap: Pretty Heatmaps version 1.0.12 from CRAN. 2019.
41. Cantalapiedra CP, Hernández-Plaza A, Letunic I, Bork P, Huerta-Cepas J. eggNOG-mapper v2: Functional Annotation, Orthology Assignments, and Domain Prediction at the Metagenomic Scale. Mol Biol Evol. 2021;38(12):5825-5829.
42. Coudert E, Gehant S, de Castro E, Pozzato M, Baratin D, Neto T, et al. Annotation of biologically relevant ligands in UniProtKB using ChEBI. Bioinformatics. 2023;39(1):btac793.
43. Yu G, Wang L, Han Y, He Q. clusterProfiler: an R Package for Comparing Biological Themes Among Gene Clusters. Omics. 2012;16(5):284-287.
44. Mu H, Chen J, Huang W, Huang G, Deng M, Hong S, et al. OmicShare tools: A zero-code interactive online platform for biological data analysis and visualization. Imeta. 2024;3(5):e228.

TABLES

Table 1 Mapping statistics for RNA-seq samples.

Sample	Input Reads	Uniquely Mapped (%)	Multi Mapped (%)	Unmapped (Too Short) (%)	Avg.Mapped Length (bp)
SS1_1	49808246	85.02	7.71	7.17	147.74
SS1_2	47966750	84.92	7.81	7.16	148.05
SS1_3	47136114	84.96	7.82	7.11	147.76
SS2_1	44925770	85.17	7.42	7.28	147.85
SS2_2	50334162	85.02	7.38	7.47	147.97
SS2_3	46266814	85.22	7.27	7.38	147.98
SS3_1	49608826	84.7	7.84	7.34	147.58
SS3_2	43959582	84.79	7.88	7.21	148.87
SS3_3	50813238	85.04	7.75	7.1	148.17

Table 2 BUSCO assessment of Helixer-predicted protein sequences

Category	Number	Percentage (%)
Complete BUSCOs (C)	1,498	92.80%
Single-copy (S)	1,409	87.30%
Duplicated (D)	89	5.50%
Fragmented BUSCOs (F)	25	1.50%
Missing BUSCOs (M)	91	5.60%
Total BUSCO groups (n)	1,614	-

Table 3 Functional annotation and PFAM domains of the 11 candidate genes under salt stress.

Gene_ID	Description	PFAMs	Expression under salt stress
chr2_001401.1	gag-polypeptide of LTR copia-type	Retrotran_gag_2, Retrotran_gag_3, Retrotrans_gag, gag_pre-integrs, rve	up
chr2_003131.1	phosphoenolpyruvate carboxylase	PEPcase	up
chr3_000195.1	belongs to the protein kinase superfamily	Pkinase,Pkinase_Tyr	up
chr4_002858.1	regulation of photoperiodism, flowering	bZIP_1	up
chr6_000414.1	Belongs to the RNase T2 family	Ribonuclease_T2	up
chr8_000327.1	Phosphoglycerate kinase	PGK	up
chr2_000708.1	Converts zeaxanthin into antheraxanthin and subsequently violaxanthin	FAD_binding_3, FHA, NAD_binding_8	down
chr4_000776.1	transcription factor	AP2	down
chr5_000112.1	galactinol--sucrose	Raffinose_syn	down
chr5_001889.1	Belongs to the peroxidase family	peroxidase	down
chr7_001758.1	Belongs to the cysteine synthase cystathionine beta-synthase family	PALP	down

FIGURE LEGENDS

Fig. 1 Transcriptomic quality assessment of *S. salsa* samples under salinity treatments. **(A)** Principal component analysis (PCA) based on variance-stabilized expression values shows distinct clustering of SS1 (0 mM NaCl), SS2 (200 mM), and SS3 (400 mM) samples. **(B)** Heatmap of the top 1,000 most variable genes reveals consistent within-group clustering. **(C)** Sample-to-sample Pearson correlation matrix illustrates high reproducibility among replicates. **(D)** Boxplot of normalized gene expression across samples. PCA grouping was further supported by PERMANOVA ($R^2 = 0.738$, $p = 0.007$), as detailed in Supplementary Table S2.

Fig. 2 Transcriptional response of *S. salsa* to salinity stress. **(A)** Heatmap of 5,380 unique differentially expressed genes (DEGs) identified from the union of SS2 vs SS1 and SS3 vs SS1 comparisons. Variance-stabilized and z-score normalized expression values are shown. Genes were ordered by average $\log_2$ fold change. Clustering reveals distinct transcriptional profiles across salinity treatments. **(B)** Venn diagram illustrating the overlap of DEGs among three salinity treatment comparisons (SS2 vs SS1, SS3 vs SS1, and SS3 vs SS2) in *S. salsa*. A total of 462 DEGs were identified as common to all three comparisons. **(**C**)** Gene Ontology (GO) enrichment analysis of the shared DEGs. The top 20 significantly enriched GO terms are shown, categorized into Biological Process, Cellular Component, and Molecular Function. Bar lengths indicate the number of genes associated with each GO term.

Fig. 3 Expression patterns of key salt-responsive genes in *S. salsa* under increasing salinity. **(A–F)** Six genes significantly upregulated in response to increasing NaCl concentrations (0, 200, and 400 mmol/L). **(G–K)** Five genes significantly downregulated under salinity stress. Gene expression values are shown as normalized counts (mean ± SEM, n = 3). Statistical significance was assessed using one-way ANOVA followed by multiple comparisons. Significant differences among treatment groups are indicated by asterisks: $p < 0.05$ (*), $p < 0.01$ (**), $p < 0.001$ (***). All upregulated genes show monotonic increases, while all downregulated genes exhibit consistent suppression under rising salinity conditions, indicating their potential regulatory roles in *S. salsa* salt stress adaptation.

Fig. 4 KEGG pathway–gene network of selected differentially expressed genes.
The network illustrates the associations between KEGG pathways (purple nodes) and input genes (pink nodes). Node size represents the number of connections (degree), and edges indicate known functional relationships based on KEGG pathway annotation. Larger pathway nodes correspond to more genes involved in the respective biological processes

Fig. 1

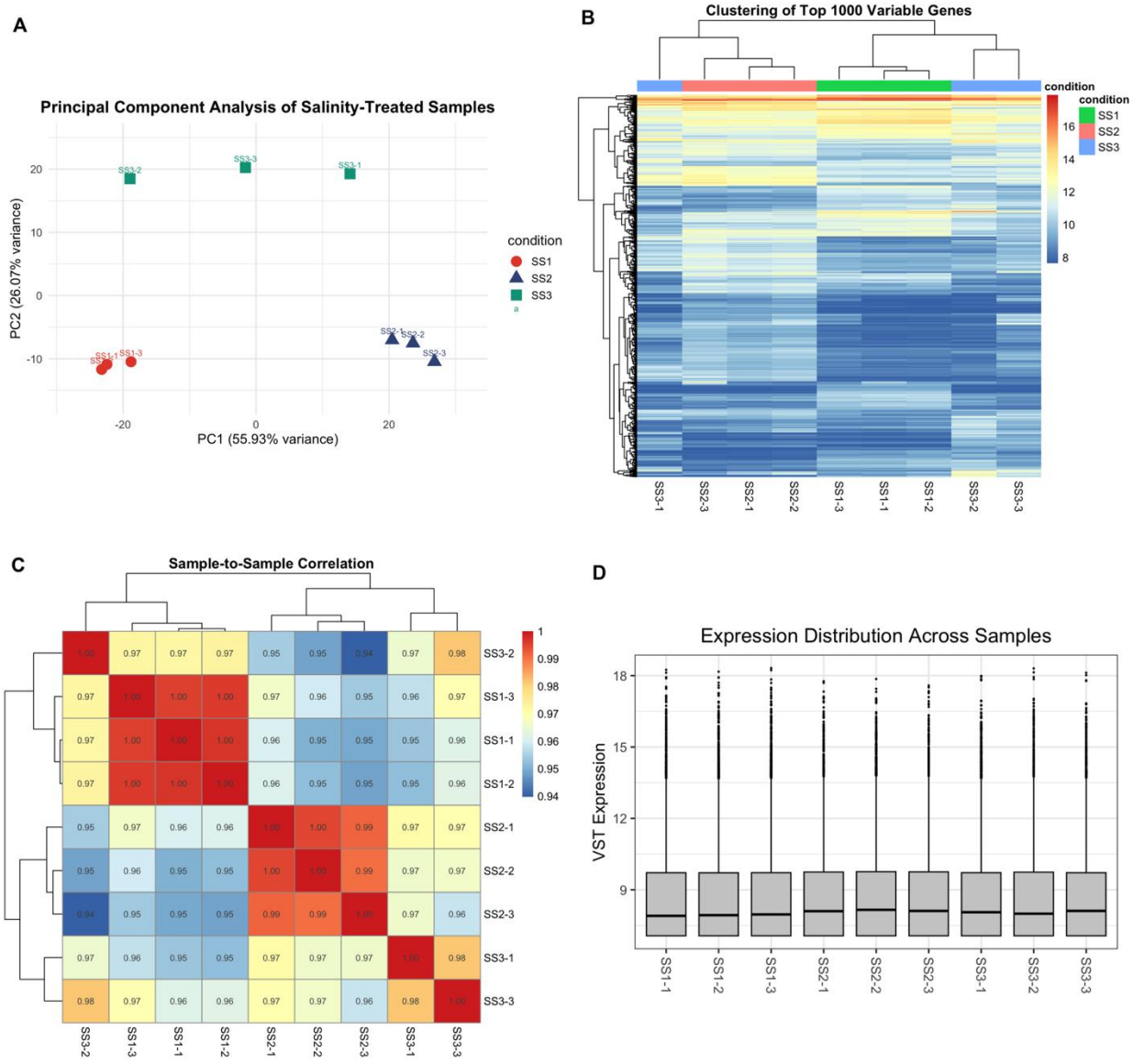
A
Principal Component Analysis of Salinity-Treated Samples
PC2 (26.07% variance)
PC1 (55.93% variance)
condition
SS1
SS2
SS3
B
Clustering of Top 1000 Variable Genes
condition
C
Sample-to-Sample Correlation
D
Expression Distribution Across Samples
VST Expression

Fig. 2

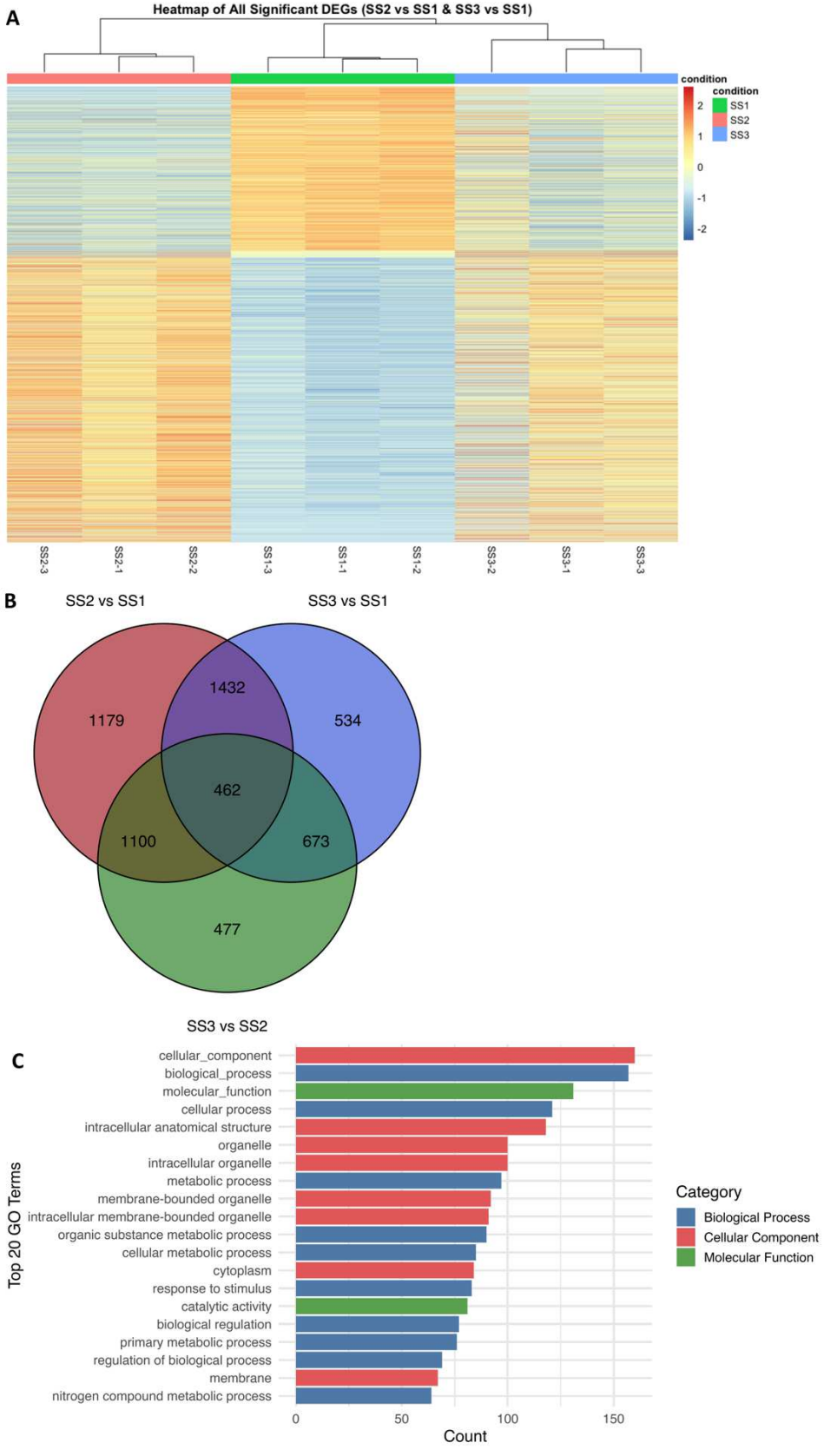
A
Heatmap of All Significant DEGs (SS2 vs SS1 & SS3 vs SS1)
condition
SS1
SS2
SS3
2
1
0
-1
-2
SS2-3
SS2-1
SS2-2
SS1-3
SS1-1
SS1-2
SS3-2
SS3-1
SS3-3
B
SS2 vs SS1
SS3 vs SS1
1179
1432
534
462
1100
673
477
C
SS3 vs SS2
cellular_component
biological_process
molecular_function
cellular process
intracellular anatomical structure
organelle
intracellular organelle
metabolic process
membrane-bounded organelle
intracellular membrane-bounded organelle
organic substance metabolic process
cellular metabolic process
cytoplasm
response to stimulus
catalytic activity
biological regulation
primary metabolic process
regulation of biological process
membrane
nitrogen compound metabolic process
Top 20 GO Terms
0
50
100
150
Count
Category
Biological Process
Cellular Component
Molecular Function

Fig. 3

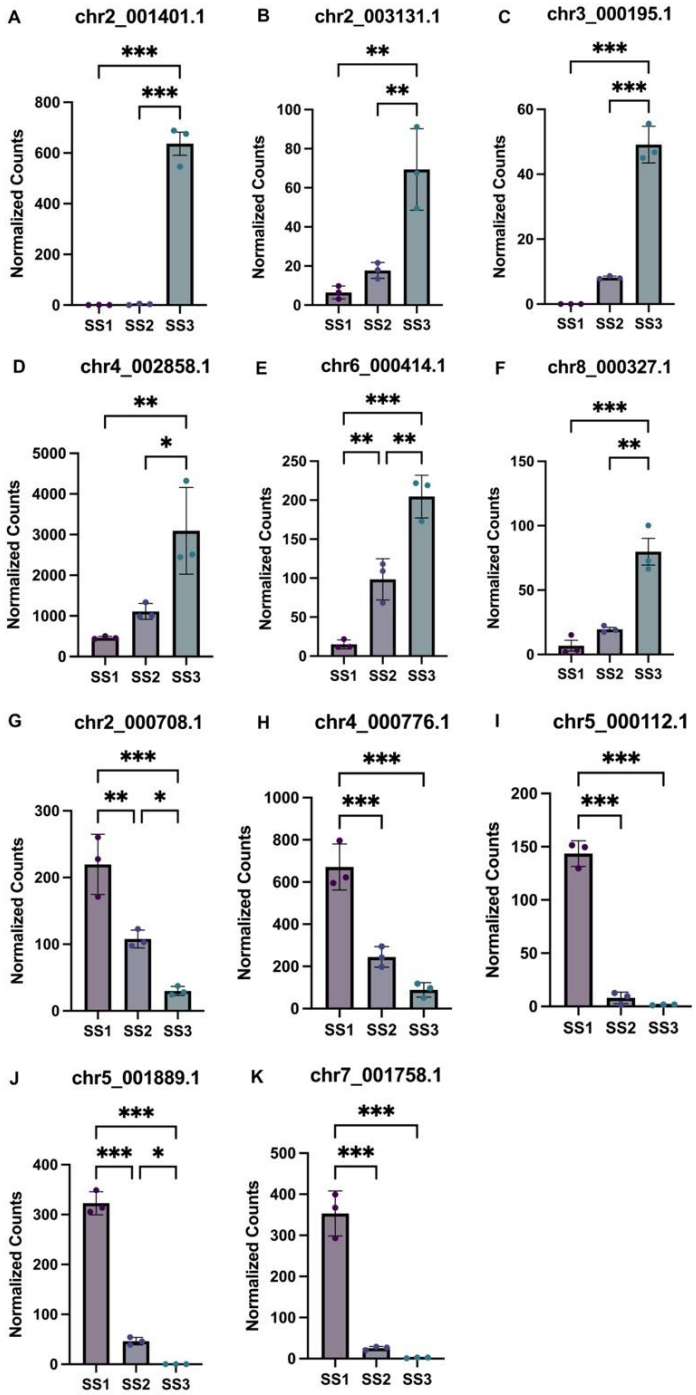
A
chr2_001401.1
B
chr2_003131.1
C
chr3_000195.1
D
chr4_002858.1
E
chr6_000414.1
F
chr8_000327.1
G
chr2_000708.1
H
chr4_000776.1
I
chr5_000112.1
J
chr5_001889.1
K
chr7_001758.1
Normalized Counts
SS1
SS2
SS3

Fig. 4

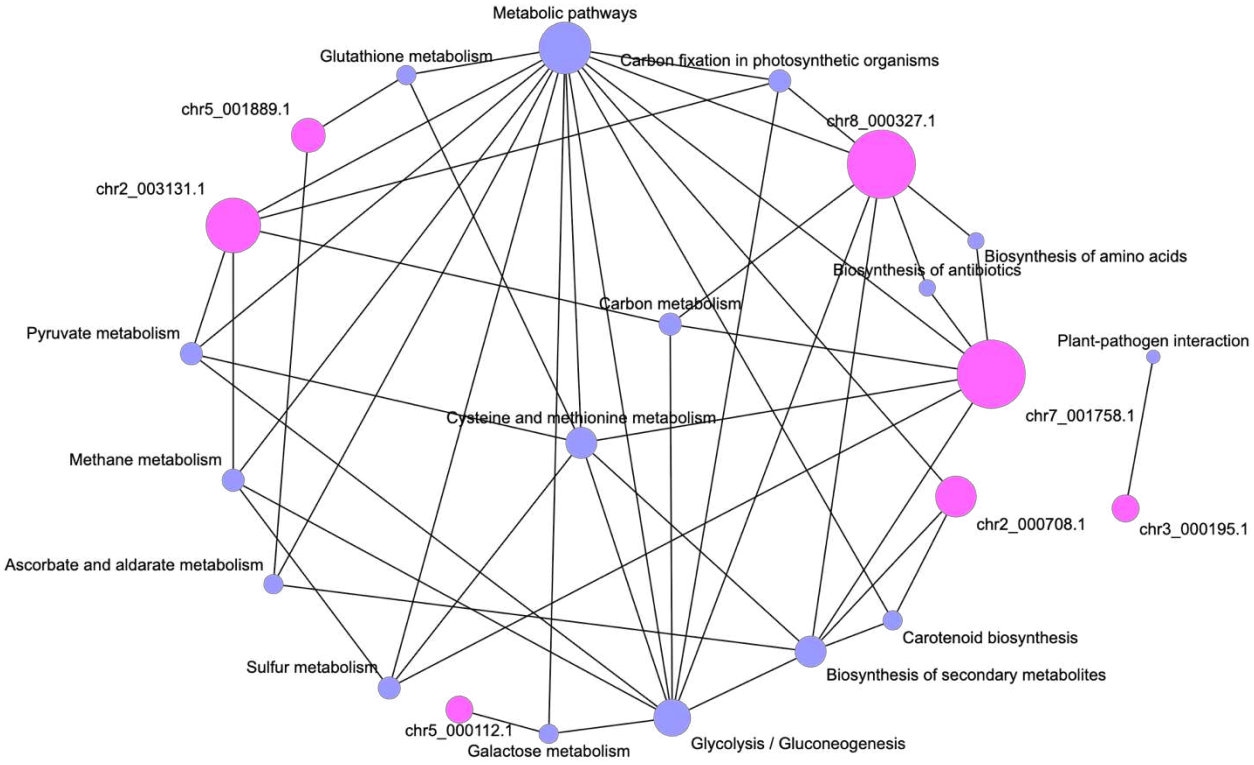
Metabolic pathways
Glutathione metabolism
Carbon fixation in photosynthetic organisms
chr5_001889.1
chr8_000327.1
chr2_003131.1
Biosynthesis of amino acids
Biosynthesis of antibiotics
Carbon metabolism
Pyruvate metabolism
Plant-pathogen interaction
chr7_001758.1
Cysteine and methionine metabolism
Methane metabolism
chr2_000708.1
chr3_000195.1
Ascorbate and aldarate metabolism
Carotenoid biosynthesis
Sulfur metabolism
Biosynthesis of secondary metabolites
chr5_000112.1
Galactose metabolism
Glycolysis / Gluconeogenesis

Supplementary Files

This is a list of supplementary files associated with this preprint. Click to download.

- TableS1.RNASequencingDataStatistics.csv
- TableS2.PERMANOVAAnalysisResults.csv
- TableS3.SignificantDEGsSS2vsSS1.csv
- TableS4.SignificantDEGsSS3vsSS1.csv
- TableS5.SignificantDEGsSS3vsSS2.csv